Advances in Science and Technology Research Journal

Advances in Science and Technology Research Journal, 2026, 20(5), 159–170
https://doi.org/10.12913/22998624/215542
ISSN 2299-8624, License CC-BY 4.0

Received: 2025.11.27
Accepted: 2026.03.15
Published: 2026.04.01

Synthesis and properties of surface-modified chitosan magnetic nanoparticles

Katarzyna Winiarczyk[1], Agnieszka Surowiec[2], Zbigniew Surowiec[1*]

[1] Institute of Physics, Maria Curie-Sklodowska University, Pl. Marii Curie-Skłodowskiej 1, 20-031 Lublin, Poland
[2] Faculty of Management, Lublin University of Technology, ul. Nadbystrzycka 38, 20-618 Lublin, Poland
* Corresponding author e-mail: zbigniew.surowiec@mail.umcs.pl

ABSTRACT

The search for new methods of synthesising magnetic nanoparticles is crucial because the properties of these materials are extremely sensitive to the way they are obtained. Innovative synthesis techniques allow these parameters to be precisely controlled, which translates into the ability to design nanoparticles with precisely tailored functions. This is important for both technological and biomedical applications. New methods can also increase production efficiency and repeatability, reduce the toxicity of reagents, and enable the production of nanomaterials with previously unavailable properties. This study attempted to synthesise chitosan-functionalised magnetite nanoparticles in an innovative way using ultrasound. The aim of the study was to compare the structural, magnetic and calorimetric properties of nanoparticles synthesised by co-precipitation and by a new modified method using ultrasound. In addition, the effect of the amount of chitosan on the physical properties of the nanoparticles was examined. The structure and morphology of the obtained nanoparticles were characterised by X-ray diffraction and transmission electron microscopy, determining their average sizes and size distributions. The effect of the amount of surfactant and the method of nanocrystal synthesis on the magnetic properties was analysed using Mössbauer spectroscopy, while calorimetric measurements demonstrated the suitability of magnetite nanoparticles with a chitosan-modified surface for potential hyperthermia applications. Mössbauer studies have shown that an increased amount of chitosan weakens the interactions between nanoparticles, facilitating their transition to a superparamagnetic state. The samples synthesised using the new method exhibit superparamagnetic properties at lower temperatures than the samples modified by co-precipitation. Calorimetric measurements indicate better heating properties in the samples obtained using ultrasound.

Keywords: magnetite nanoparticle, superparamagnetism, co-precipitation method, magnetic fluid hyperthermia.

INTRODUCTION

Magnetic nanoparticles are currently one of the most promising areas of research at the intersection of chemistry, physics, materials engineering, and biomedical sciences. Their unique properties resulting from a combination of quantum effects, large specific surface area, and the ability to control particle behaviour using a magnetic field – open the door to the applications that, just a few years ago, remained only in the realm of theoretical considerations. Contemporary nanotechnology uses magnetic nanoparticles in, among other things, magnetic resonance imaging, targeted therapy, magnetic hyperthermia, drug delivery systems, catalysis, environmental purification, and the construction of smart materials [1–8]. The growing interest in these structures stems not only from their versatility, but also from the possibility of precisely modifying their physicochemical properties, which allows them to be adapted to specific application tasks [9].

One of the key aspects of work on magnetic nanoparticles is the control of their stability, biocompatibility, and functionality [10, 11]. Raw, unmodified nanoparticles often tend to agglomerate, may undergo oxidation, or exhibit limited biocompatibility, which reduces their usefulness

in aquatic or biological environments. Therefore, it is important to develop the methods for modifying their surface, especially with organic substances that act as stabilisers, protective agents, or functional coatings that enable further chemical or biological activation. Such surface modifications may include both small organic ligands and natural or synthetic polymers that give nanoparticles the desired properties, from increased colloidal stability to the ability to attach biomolecules, drugs, or fluorescent markers [12–13].

Chitosan, a natural polysaccharide obtained through the deacetylation of chitin, is of particular importance in this context. Owing to its biocompatibility, non-toxicity, biodegradability, and the presence of amino functional groups, chitosan is an ideal candidate for coating magnetic nanoparticles. The chitosan layer not only stabilises the nanoparticles in solution and protects them from adverse changes, but also allows for the easy introduction of additional functions, such as the attachment of targeting ligands, drugs, or antibodies. As a result, chitosan-coated nanoparticles are widely used in medicine, including in drug delivery systems, where their surface can be designed to respond to specific stimuli or target specific cells [14–16]. In addition, chitosan, due to its antibacterial properties and gelling ability, has the potential to create smart hybrid materials that combine magnetic functions with biological activity. Therefore, the search for new techniques for the synthesis of surface-modified magnetic nanoparticles is crucial for many reasons, which result both from the limitations of the methods used so far and from the growing application requirements for nanostructured materials. The aim of this work was to compare the physical properties of magnetic nanoparticles synthesised using different techniques.

EXPERIMENT

Synthesis of magnetite nanoparticles

Synthesis of chitosan-modified nanoparticles by co-precipitation

Magnetite nanoparticles were prepared by weighing appropriate amounts of $FeSO_4$ and $Fe_2(SO_4)_3$ in a molar ratio of 1:2 and dissolving them in distilled water. Next, the mixture of aqueous solutions of Fe(II) and Fe(III) ions was added dropwise to a previously prepared ammonium base solution (pH=11). The synthesis was carried out at room temperature, and the solution was stirred vigorously (500 rpm). In order to remove oxygen, the aqueous solutions were flushed with a stream of nitrogen. The resulting precipitate was rinsed four times with distilled water. A previously prepared chitosan solution (0.1 g of chitosan dissolved in 15 ml of a 2% acetic acid) was added in small portions to the rinsed precipitate and stirred vigorously (500 rpm). Two further syntheses were carried out in the same way using chitosan weights of 0.05 g and 0.15 g. The samples are denoted CS 05, CS 10, and CS 15, respectively.

Preparation of chitosan-modified nanoparticles using ultrasound

In the first stage of synthesis, 0.1 g of chitosan was dissolved in 15 ml of a 2% CH_3COOH solution under the action of a magnetic stirrer (500 rpm) for approximately 20 minutes. Next, appropriate amounts of iron salts $FeSO_4$ and $Fe_2(SO_4)_3$ (mole ratio 1:2) were dissolved in distilled water. The oxygen removal procedure was the same as in the previous case. The next stage of synthesis took place in an ultrasonic bath (POLSONIC 310 W). The mixed solutions of iron II and III ions were added in small portions to the chitosan solution under ultrasonic agitation. Next, small portions of ammonium hydroxide solution (20 ml, pH=11) were added to the mixture. The precipitate obtained as a result of the synthesis was subjected to sedimentation using a neodymium magnet, the supernatant was removed, and the residue was rinsed with distilled water. The precipitate was left to dry. Two more samples were prepared in the same way, using chitosan weights of 0.05 g and 0.15 g, respectively. The samples were designated US CS 05, US CS 10, and US CS 15, respectively.

Characterisation

The average particle diameter was determined with use of the Williamson-Hall method from X-ray diffraction (XRD) measurement. The XRD pattern was obtained with a Philips X'Pert using a diffractometer with CuKα radiation at room temperature. Nanoparticle imaging was performed using a FEI Transmission Electron Microscope, model Tecnai G2 X-TWIN. All measurements were performed using a lanthanum cathode at a voltage of 200 kV. Samples were prepared

on copper grids coated with an amorphous carbon coating. The samples with a modified and unmodified surface were investigated with Fourier Transform Infrared Spectroscopy using the attenuated total reflection technique (FTIR-ATR). The spectra were recorded by means of a Nicolet 6700 (Thermo Scientific) spectrometer equipped with Smart Orbit ATR accessory (Thermo Scientific) in the range of 400–4000 cm^{-1} with the resolution of 4 cm^{-1}, scan velocity 0.6329, and maximum source aperture. Interferograms of 256 scans were averaged for each spectrum. The spectra were corrected by application of a suitable baseline and Advanced ATR correction function implemented within Omnic software.

Moreover, the sample was examined with Mössbauer Spectroscopy in a wider temperature range. All Mössbauer spectra were recorded in the transmission mode using a constant acceleration POLON spectrometer. The low-temperature data were obtained with the sample mounted in a 4 K Closed Cycle Refrigerator System from Janis and SHI (Woburn, MA). A ^{57}Co source in a Rh matrix and α-Fe standard were used.

RESULTS AND DISCUSSION

Chitosan-modified magnetite nanoparticle samples were tested for structural and morphological properties. The results of XRD measurements for chitosan-modified nanoparticles without the use of ultrasound are shown in Figure 1a, and the spectra obtained for the samples synthesised using an ultrasonic bath are shown in Figure 1b. A theoretical diffractogram profile (black solid line) was fitted to the experimental data and Miller indices *hkl* were marked. Analysis of the diffractograms confirms the presence of magnetite in all prepared samples. This is confirmed by the analogous distribution of diffraction peaks on the diffractograms of the samples, described by Miller indices, which are identical to that characterising magnetite. The intensities and half-widths of the reflections within the series under consideration are also similar, indicating similar crystallite sizes.

On the basis of the measured diffractograms, the average sizes of nanoparticles in each sample were determined, along with the lattice constants and strain (Table 1). The lattice parameters are almost identical for all samples and range from 8.357 Å to 8.361 Å. These values are also close to the lattice constant of magnetite, which is 8.397 Å [17].

In the case of medium-sized crystallites, higher values are observed for the nanoparticles prepared and modified under the influence of ultrasound, amounting to approximately 14 nm. Slightly smaller sizes (approx. 11 nm) were achieved by the crystallites synthesised by co-precipitation and modified with chitosan after the crystal growth stage. There are noticeable differences in the values of lattice strains, which are

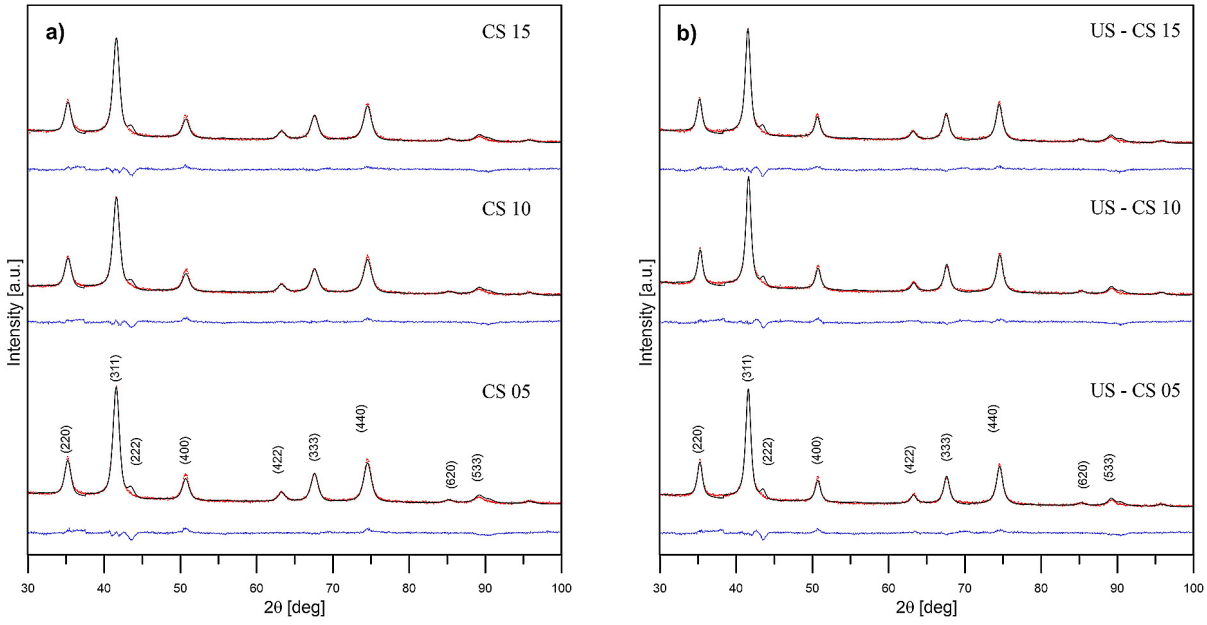

Figure 1. Diffractograms of samples modified with chitosan (a) synthesised by co-precipitation, (b) prepared using ultrasound

Table 1. Parameters of crystal structure of chitosan-modified magnetite nanoparticle (a – lattice constant, d – average nanoparticle size, η – lattice strain)

Sample	*a* (Å)	*d* (nm)	*η*
CS 05	8.358 ± 0.001	11.0 ± 0.2	0.253 ± 0.005
CS 10	8.361 ± 0.001	10.5 ± 0.2	0.247 ± 0.004
CS 15	8.360 ± 0.001	10.9 ± 0.2	0.269 ± 0.005
CS US 05	8.357 ± 0.001	13.7 ± 0.2	0.064 ± 0.005
CS US 10	8.358 ± 0.001	14.2 ± 0.2	0.079 ± 0.006
CS US 15	8.358 ± 0.001	13.7 ± 0.2	0.086 ± 0.005

lower for the samples prepared with ultrasound and range from 0.064 to 0.086. The samples obtained by coprecipitation are characterised by approximately three times higher lattice strains.

The structures imaged using a transmission electron microscope are presented in Figures 2 and 3. Qualitative analysis shows no significant changes in the entire series in terms of nanoparticle structure or dispersion, regardless of the use of ultrasound during synthesis. The shape of the obtained nanoparticles is mostly spherical. The crystals tend to aggregate and overlap.

On the basis of TEM images, an analysis of the size distribution of nanoparticles and their standard deviations was also performed. The size distributions are illustrated by the histograms in Figure 4. The distribution parameters were calculated assuming a log-normal distribution according to the formula:

$$P(d) = \frac{1}{x\sigma_d\sqrt{2\pi}} exp\left(-\frac{d^2}{2\sigma_d^2}\right) \quad (1)$$

where: $d = ln\frac{x}{x_0}$, σ_d is the standard deviation d and x_0 is the average size of a nanoparticle.

On the basis of these results, it can be concluded that in the case of the samples prepared in a standard manner (i.e., without the use of ultrasound), the spread of crystallite sizes is greater than in the case of synthesis using ultrasound, and the nanoparticles reach sizes in the range of 5 nm to 17 nm, with extreme values accounting for a small proportion. The exception is the sample modified with 0.1 g of chitosan (CS 10) - the average size of nanoparticles ranges from 5 nm to 14 nm, and the probability of extreme values occurring is higher than in other preparations. The use of ultrasound during synthesis results in a reduction in the size distribution of nanoparticles for samples US CS 05 and US CS 15. For sample US CS 10, the distribution of average sizes is greater (nanoparticles reach sizes ranging from 5 nm to 18 nm). Table 2 summarises the parameters determined from TEM images. The average sizes of nanoparticles within the entire series are similar and range from approximately 9 nm to 11 nm. It can therefore be concluded that ultrasonic synthesis does not have a significant effect on the size of crystallites, but rather on the spread of their sizes.

When comparing the average crystal sizes to those determined by X-ray diffraction, it can be seen that they are slightly smaller (this applies to both samples without and with ultrasound). This is due to the characteristics of both methods.

In order to obtain the information on how chitosan molecules bind to the surface of magnetite nanoparticles, the samples studied were examined using infrared spectroscopy. The spectra were measured at room temperature. Figure 5a) presents the measurement results for: pure chitosan, magnetite nanoparticles, and the chitosan-coated samples obtained by the classic co-precipitation method. All spectra of chitosan-coated nanoparticles are characterised by a broad and intense band extending between 3600 cm^{-1} and 3100 cm^{-1}, corresponding to N–H and O–H stretching vibrations. The bands characteristic of the chitosan molecule are also noticeable: at 2920 cm^{-1} and 2860 cm^{-1} –CH stretching vibrations (least intense for the sample with 0.05 g of chitosan); at 1647 cm^{-1} stretching vibrations of C=O of primary amide, at 1374 cm^{-1} stretching vibrations of C–N of tertiary amide and a band at 1589 cm^{-1} – bending vibrations of N–H (primary amine). Additionally, around 600 cm^{-1}, the band typical for Fe–O vibrations in iron oxides begins to appear. These results indicate a permanent binding of chitosan on the surface of magnetite nanoparticles.

In the case of synthesis and surface modification in the presence of ultrasound (Figure 5b), the presence of the above-mentioned absorption bands is

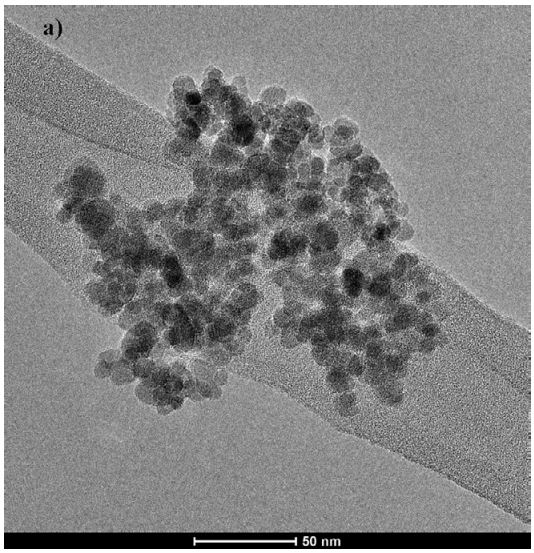

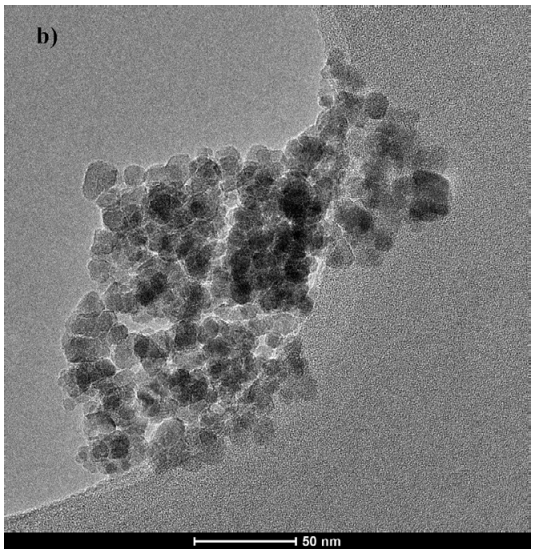

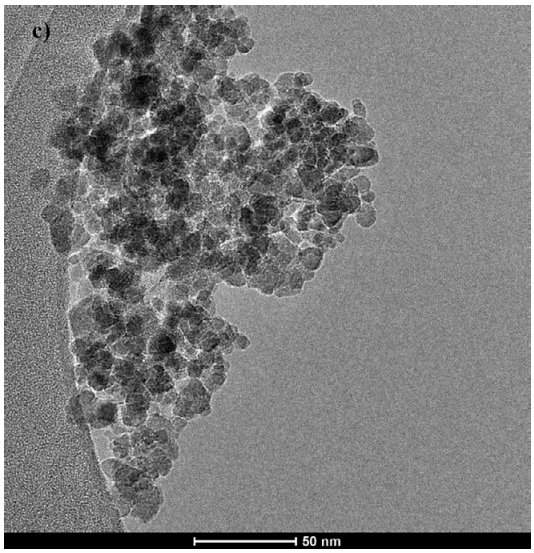

Figure 2. TEM images of chitosan-coated nanoparticles (a) CS 05, (b) CS 10 and (c) CS 15 obtained by co-precipitation

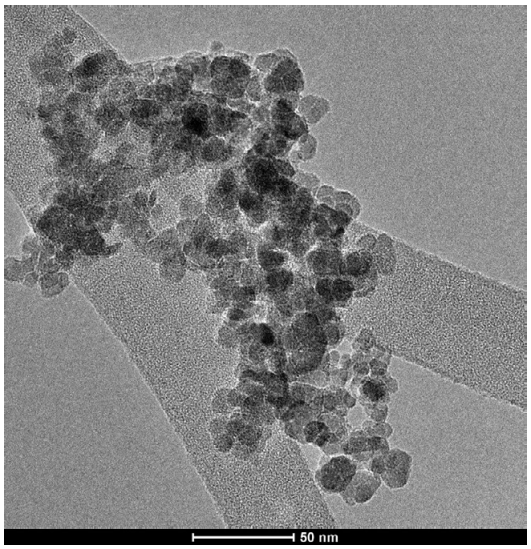

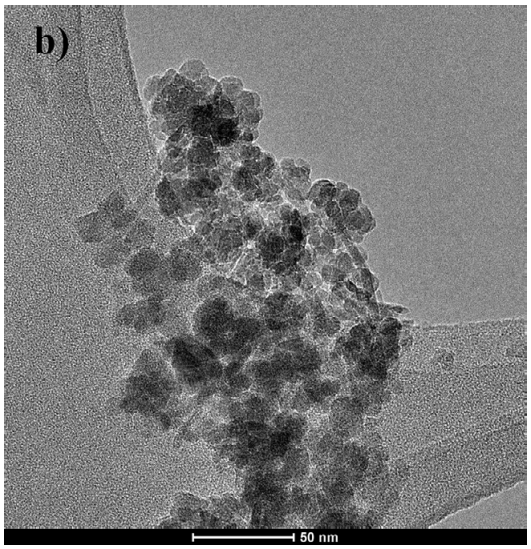

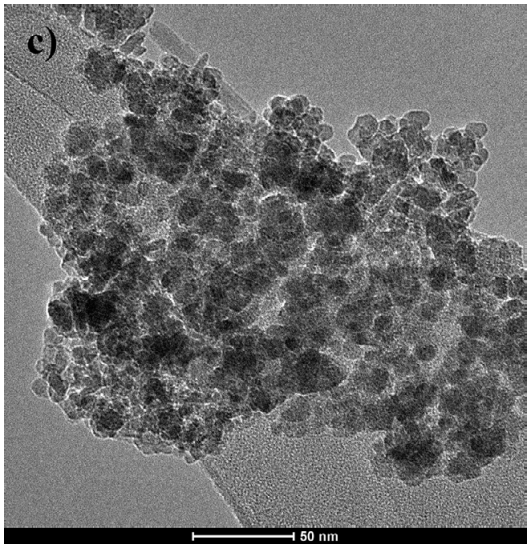

Figure 3. TEM images of chitosan-coated nanoparticles (a) US CS 05, (b) US CS 10 and c) US CS 15 synthesised with the use of ultrasound

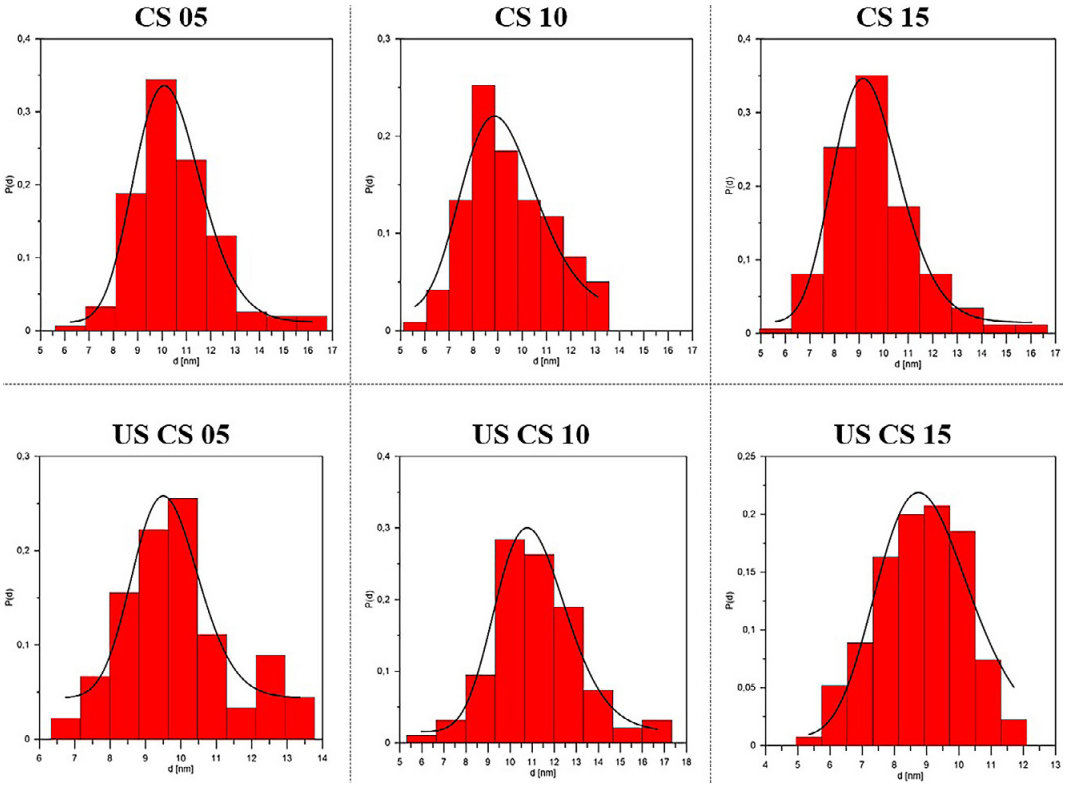

Figure 4. Histograms of size distribution for chitosan-modified samples

Table 2. Sample parameters determined based on TEM data

sample	d [nm]	Δd [nm]	σ [nm]	$\Delta\sigma$ [nm]
CS 05	10.27	0.07	0.134	0.008
CS 10	9.13	0.22	0.172	0.041
CS 15	9.36	0.07	0.146	0.009
US CS 05	9.59	0.14	0.098	0.019
US CS 10	11.01	0.10	0.147	0.012
US CS 15	8.98	0.15	0.163	0.027

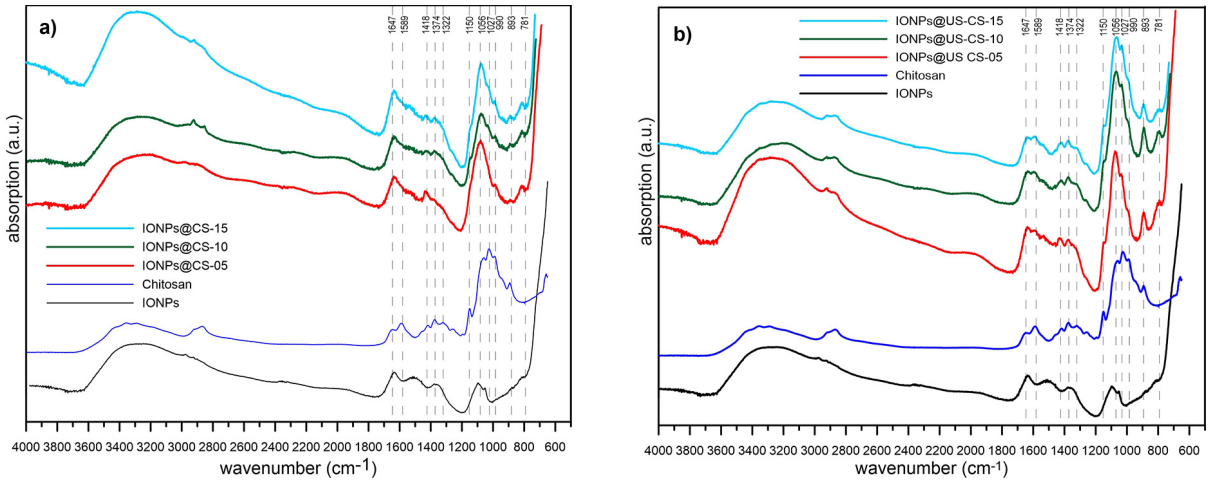

Figure 5. IR spectra of chitosan-modified magnetite nanoparticles: (a) synthesised by co-precipitation, (b) in the presence of ultrasound

also noted. A visible difference is observed in their intensity. The CH vibration bands (2920 cm^{-1} and 2860 cm^{-1}) and the bands around 1056 cm^{-1} (C–O stretching vibrations) are more intense, while the C=O stretching vibration absorption bands (1647 cm^{-1}) are less intense [18–19]. This regularity is observed for any amount of chitosan used for synthesis. It can therefore be concluded that synthesis with the use of ultrasound increases the intensity of the above-mentioned absorption bands. The magnetite nanoparticles modified with chitosan were characterised in terms of phase composition, crystallite size, crystallite size distribution width, and tested for the binding of organic molecules on the surface of magnetite nanoparticles. The characterised systems were then measured using Mössbauer spectroscopy. The aim of this study was to determine the effect of the amount of surfactant, in this case chitosan, on the hyperfine interactions in nanoparticles, in particular on the internal magnetic fields and the ability to transition to a superparamagnetic state. The measurements were performed in the temperature range from 4K to room temperature, and the samples were in powder form. The obtained spectra are presented in Figures 6 and 7. The spectra of the samples synthesised by co-precipitation and then coated were developed using a five-component model below the Verwey transition. The spectra obtained at 150 K and above were fitted with four sextets. Two of them were assigned to the position of Fe^{3+} ions in a tetrahedral environment and the position of iron ions with an average valence of $Fe^{2.5+}$ in an octahedral environment in the magnetite unit cell. The intensity ratio of these two $Fe^{3+}/Fe^{2.5+}$ components was close to 1:2. The next two sextets were attributed to iron ions in the maghemite lattice. The spectra obtained at 200 K and room temperature contain magnetic components with a quasi-continuous distribution. These components are associated with the superferromagnetic phase. This state precedes superparamagnetic fluctuations of magnetic moments in nanoparticles [20]. However, the superparamagnetic phase itself in the nanoparticles synthesised by co-precipitation and then coated is observed in samples CS 05 and CS 10 at 290 K and 200 K, respectively. Hence, it can be concluded that a larger amount of chitosan better separates the nanoparticles, weakening the intermolecular dipole interaction, which makes it difficult to overcome the energy barrier and transition to the superparamagnetic state. The spectra of the samples produced and coated using ultrasound appear to be more complex. They were developed using a larger number of magnetic components than the spectra of nanoparticles obtained by the classical co-precipitation method. The components were not clearly assigned to the corresponding iron ions in the crystallographic lattice. However, the average value of the superfine magnetic field was determined for all tested samples. The dependence of B_{hf} on temperature is shown in Figure 8. At low temperatures, the field values are similar in each tested sample. At room temperature, the lowest B_{hf} value was recorded for the US CS 10 sample.

Figure 9 shows the dependence of the superparamagnetic phase fraction on temperature for the chitosan-coated nanoparticles. The studies indicate that the largest increase in the superparamagnetic phase is observed in the samples synthesised with the use of ultrasound. This result may be somewhat surprising, as nanoparticles obtained with the use of ultrasound are larger (approx. 14 nm) than nanoparticles obtained by the classic co-precipitation method (approx. 10.5 nm), and one would expect a higher proportion of the superparamagnetic phase in smaller nanoparticles. Therefore, the values of the hyperfine interaction parameters in surface-modified nanoparticles are influenced not only by the size of the nanoparticles or the type of coating enveloping the magnetic core, but also by the method of coating the nanoparticle surface with a surfactant and the way in which the organic coating bonds to the nanoparticle surface.

Finally, the influence of an alternating electromagnetic field on the heat generation rate expressed in terms of the specific absorption rate (SAR) and specific loss power (SLP) was investigated experimentally. This property of nanoparticles is crucial in the application of magnetic fluid hyperthermia for medical purposes. SAR is commonly defined as:

$$SAR = \frac{P}{m_{MNP}} \tag{2}$$

where: P denotes the power generated per unit mass of nanoparticles m_{MNP}. The power generated by MNPs depends on the physical and magnetic properties of these nanoparticles. However, the dissipated power depends linearly on the frequency f, and squarely on the magnetic field strength H. To eliminate dependence on external conditions, the concept of internal loss power has become a standard approach.

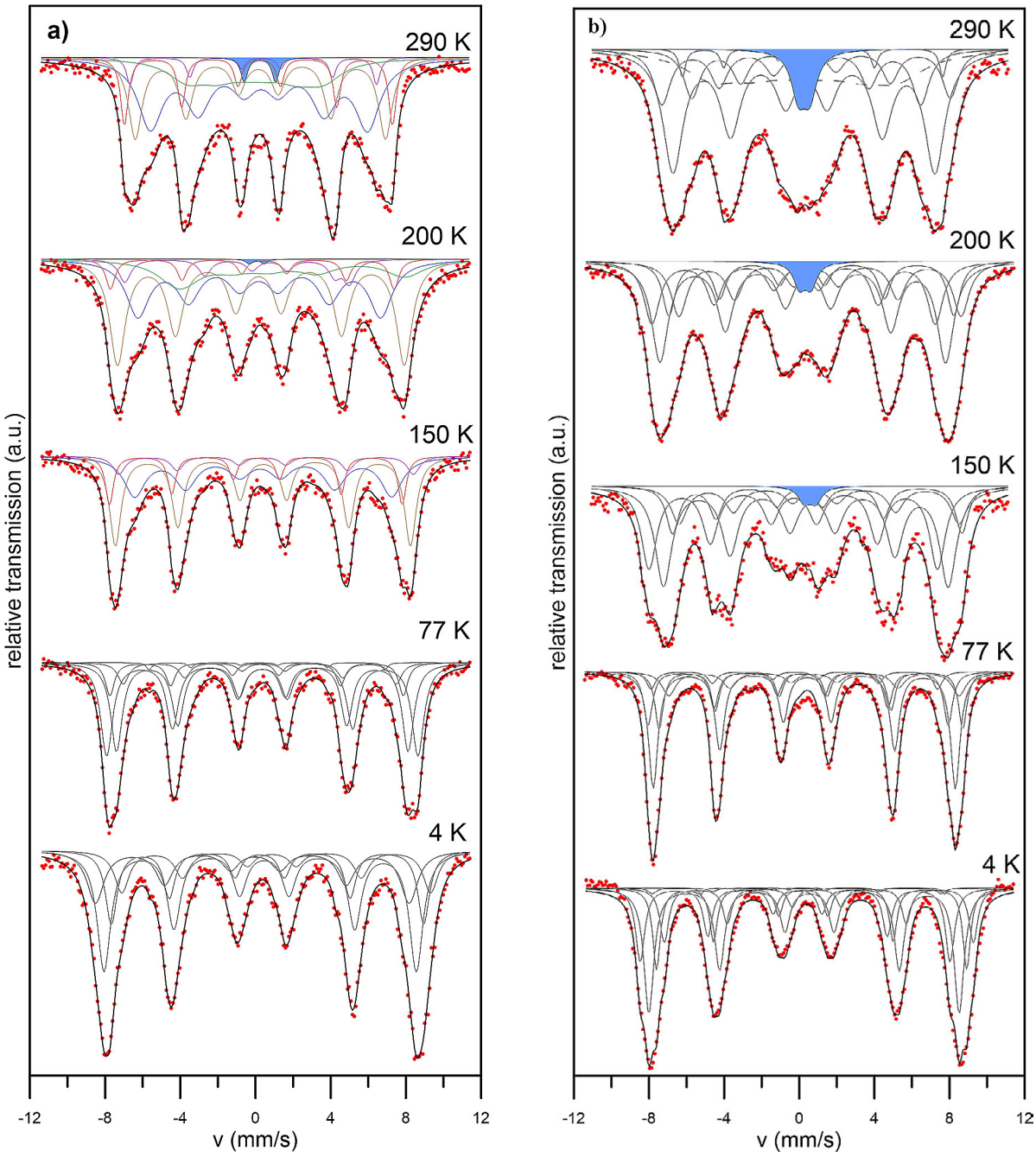

Figure 6. Mössbauer spectra of chitosan-coated magnetite nanoparticles taken at different temperatures. Sample CS 05 obtained by (a) coprecipitation, (b) coating in the presence of ultrasounds

$$ILP = \frac{SAR}{fH^2} \tag{3}$$

The measurements were carried out in an alternating magnetic field (AMF) with an intensity of H=10 kA/m and a frequency of f = 532.4 kHz. The corrected slope method was used to ensure that appropriate regions of the data are used for calculations SAR [21]. Figure 10 shows the results of calorimetric measurements of magnetic nanoparticles in AMF. By comparing the obtained relationships, it can be clearly stated that the chitosan-modified nanoparticles in the presence of ultrasound significantly improve the heating properties of the synthesised samples for each chitosan concentration. Ferrofluids reach a temperature of 62 °C in 300 seconds (or less, in the case of the US CS 10 sample). Furthermore, the use of ultrasound in the synthesis also results in a uniform and linear increase in the temperature of the samples under the influence of an alternating magnetic field, and the cooling phase (after switching off the magnetic field) occurs

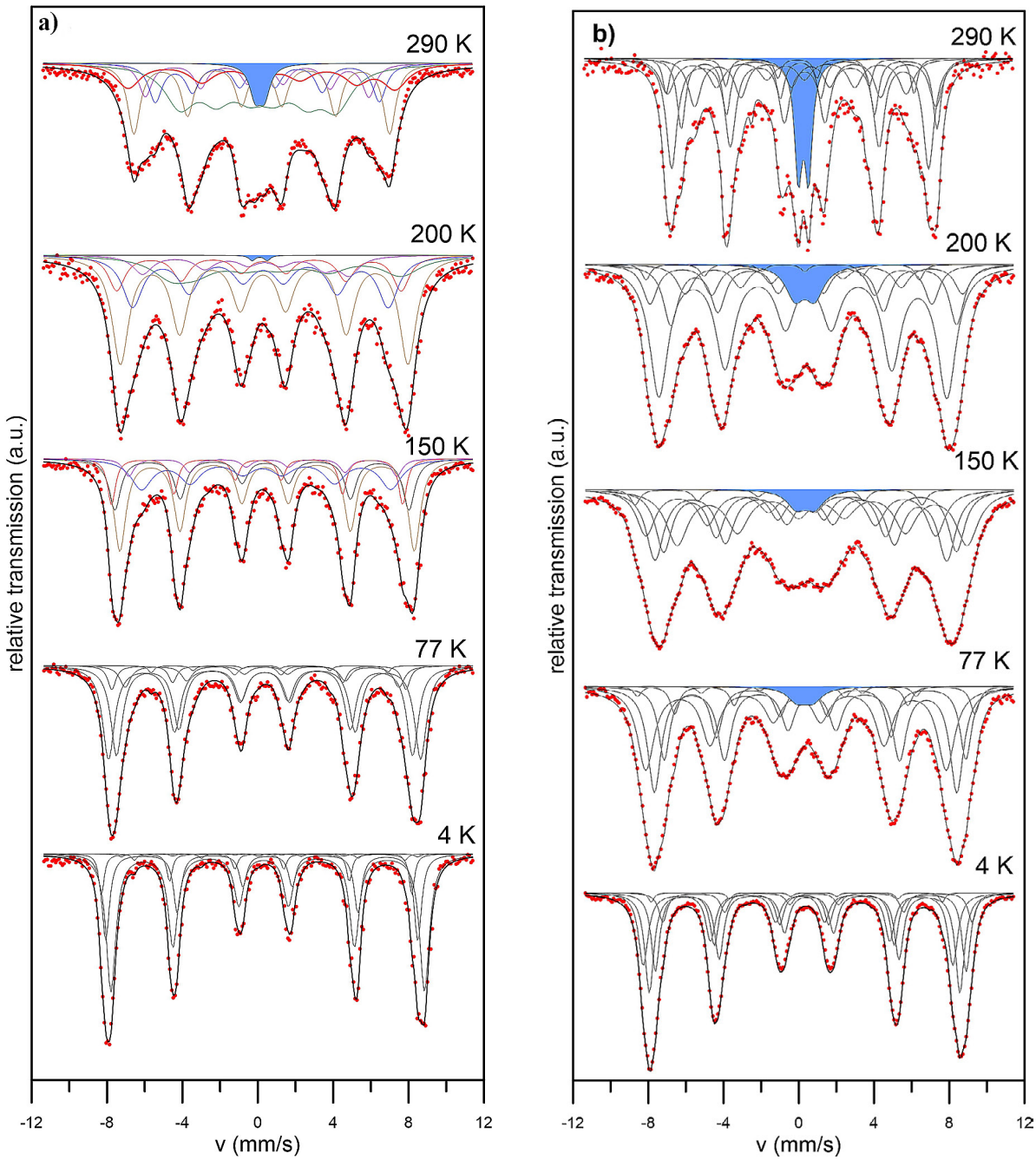

Figure 7. Mössbauer spectra of chitosan-coated magnetite nanoparticles taken at different temperatures. Sample CS 10 obtained by (a) coprecipitation, (b) coating in the presence of ultrasounds

in a moderate and gentle manner. The samples obtained without the use of ultrasound have weaker heating properties. The temperature reached by these ferrofluids is 44 °C for the CS 05 sample and 53 °C for the other two samples, which is still the desired temperature for magnetic fluid hyperthermia, but it takes longer to reach (600 s). Furthermore, the temperature increases in the first stage of the experiment, with the magnetic field switched on, is non-linear, even irregular, and this is evident for all samples synthesised without ultrasound, although most clearly for sample CS 05. On the basis of the collected data, the SAR and ILP parameters were determined and are presented in Table 3.

The nanoparticles modified with chitosan and prepared in the presence of ultrasound exhibit high SAR and ILP values. For sample US CS 05, the specific absorption rate is 50.99 W/g, and the internal loss power is 0.370 nHm²/kg. As the amount of chitosan used to coat magnetite nanoparticles increases, the SAR and ILP

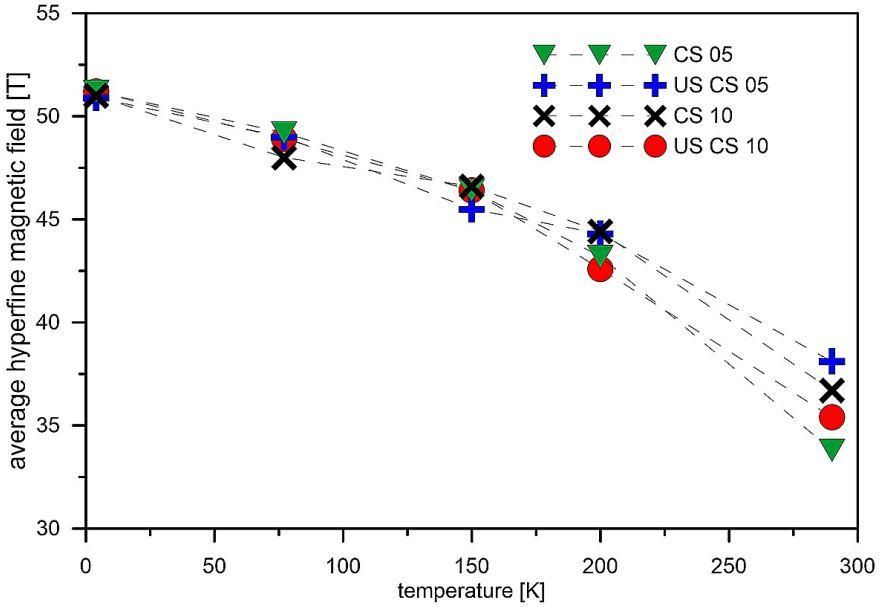

Figure 8. Dependence of the average internal magnetic field on the temperature determined for chitosan-coated nanoparticles

Table 3. SAR and ILP values and nanoparticle concentrations in chitosan-modified samples subjected to calorimetric testing

Sample	Concentration [mg/ml]	SAR [W/g]	ILP [nHm²/kg]
CS 05	4	27.08 ± 3.67	0.200 ± 0.027
CS 10	10	14.72 ± 0.59	0.110 ± 0.004
CS 15	13	12.20 ± 0.74	0.090 ± 0.005
US CS 05	10	50.99 ± 2.88	0.370 ± 0.021
US CS 10	20	40.23 ± 3.19	0.300 ± 0.023
US CS 15	20	19.13 ± 1.09	0.140 ± 0.008

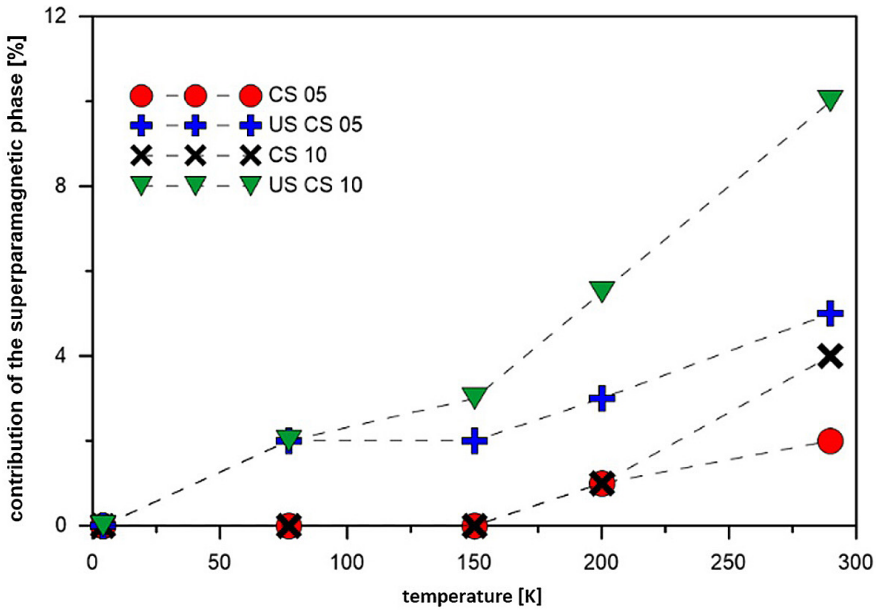

Figure 9. The dependence of superparamagnetic phase shares on temperature determined for chitosan-coated nanoparticles

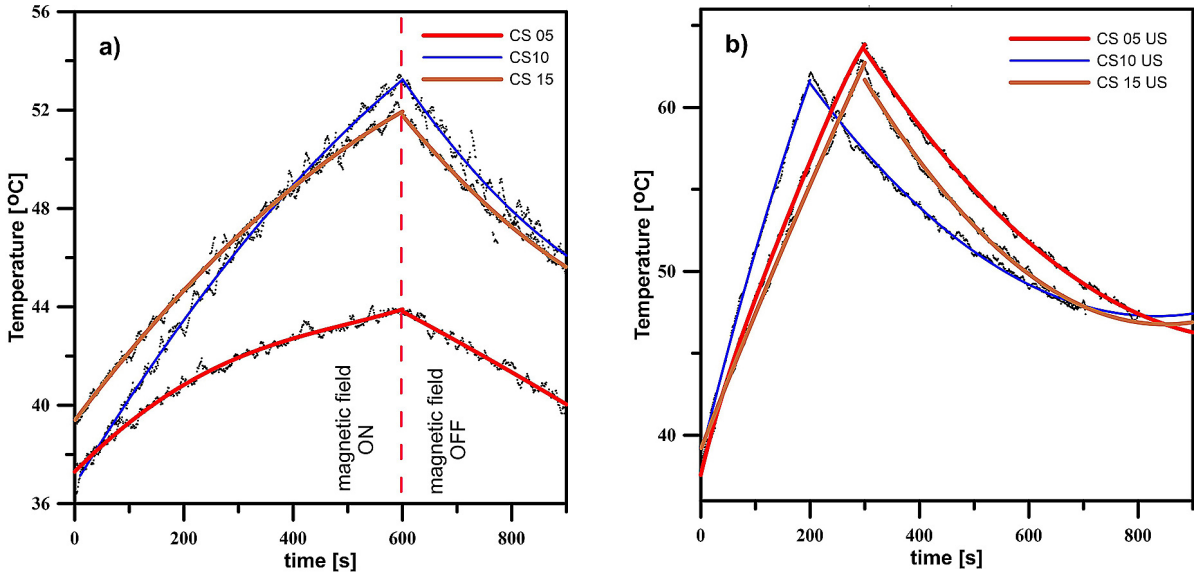

Figure 10. Temperature dependence on time for chitosan-modified samples synthesised (a) without and (b) with ultrasound

parameters decrease (even when the concentration of ferrofluids in the measured samples is the same – samples US CS 10 and US CS 15). A large amount of chitosan in the sample can cause multiple layers of chitosan molecules to form on the surface of the nanoparticles, which translates into agglomeration of the nanoparticles and, as a result, also into their ability to heat up. The samples prepared without the use of ultrasound show the same tendency. Among them, the sample with the lowest amount of chitosan used for coating (CS 05) has the highest SAR and ILP values. It seems that the amount of chitosan used for synthesis has a greater impact on the heating parameters than the concentration of individual ferrofluids.

CONCLUSIONS

The Fe_3O_4 nanoparticles obtained with the coprecipitation method were investigated in terms of their chemical and physical properties. The synthesis method was modified by using ultrasound, simultaneously precipitating nanoparticles and modifying their surface, and comparing these results with the synthesis using the classical co-precipitation method. The XRD studies showed that the average sizes of chitosan-modified nanoparticles obtained during ultrasonic synthesis are slightly larger than those obtained and modified in the standard way.

A different nature of chitosan binding on the magnetite surface was observed during synthesis in the presence of ultrasound compared to the classical coprecipitation method. The results of Mössbauer studies showed that a larger amount of surfactant used for the functionalisation of the nanoparticle surface weakens the dipole interactions between them, thus contributing to an easier transition to the superparamagnetic state. Additionally, in the case of the samples synthesised with ultrasound, the superparamagnetic component appears at lower temperatures than in the samples modified with the same amount of chitosan obtained by the standard method.

Calorimetric measurements have clearly confirmed the superior heating properties of the chitosan-coated nanoparticles prepared with ultrasound. These samples heat up faster, reaching temperatures above 60 °C, and the parameters determining the heating capacity are significantly higher than in the case of the samples obtained and modified without the use of ultrasound.

REFERENCES

1. Nqayi S., Sondezi B. Quantum size effects on magnetism in Eu_2MnHfO_6 nanoparticles: Role of surface-to-volume ratio, magnetic blocking, and magnetic phase transitions. Results in Physics 2025; 75: 108326, https://doi.org/10.1016/j.rinp.2025.108326
2. Suna C., Leeb J., Zhanga M. Magnetic nanoparticles in MR imaging and drug delivery, Adv Drug

Deliv Rev. 2008; 60(11): 1252–1265, https://doi.org/10.1016/j.addr.2008.03.018

3. Chudzik B., Miaskowski A., Surowiec Z., Czernel G., Duluk T., Marczuk A., Gagoś M. Effectiveness of magnetic fluid hyperthermia against Candida albicans cells. Int J Hyperthermia 2016; 32(8): 842–857, https://doi.org/10.1080/02656736.2016.1212277
4. Gac W., Zawadzki W., Słowik G., Kuśmierz M., Karpińska-Wlizło K., Surowiec Z. Dual role of iron in alumina supported bimetallic nickel catalysts for CO_2 methanation, Applied Surface Science 2025; 711; 164018, d https://doi.org/10.1016/j.apsusc.2025.164018
5. Orzechowska M., Rećko K., Klekotka U., Czerniecka M., Tylicki A., Satuła D., Soloviov D. V., Beskrovnyy A. I., Miaskowski A., Kalska-Szostko B. Structural and thermomagnetic properties of gallium nanoferrites and their influence on cells in vitro. International Journal of Molecular Sciences 2023; 24: 14184. https://doi.org/10.3390/ijms241814184
6. Ali A., Shah T., Ullah R., Zhou P., Guo M., Ovais M., Tan Z., Rui Y. Review on recent progress in magnetic nanoparticles: synthesis, characterization, and diverse applications. Front. Chem. 2021; 9: 629054. https://doi.org/10.3389/fchem.2021.629054
7. Mishra S., Yadav MD. Magnetic Nanoparticles: A comprehensive review from synthesis to biomedical frontiers. Langmuir 2024; 40(33): 17239–17269. https://doi.org/10.1021/acs.langmuir.4c01532
8. Rećko K., Orzechowska M., Olszewski W., Beskrovnyy A., Biernacka M., Klekotka U., Miaskowski A., Szymański K. Investigations on the enhancement of thermomagnetic properties in Fe2.4Ga0.6O4. Phase Transitions 2023; 96: 105. doi.org/10.1080/01411594.2022.2159404
9. Djellal, N., Pęczkowski, P., Mekki, D. E., Navarro, E., Tahraoui, T., Piętosa, J., Michalik, J. M., Marín, P., Gondek, Ł. Tailoring magnetic properties of Fe0.65Co0.35 nanoparticles by compositing with RE2O3 (RE = La, Nd, and Sm). Materials, 2022; 15(20): 7290. https://doi.org/10.3390/ma15207290
10. Pęczkowski P., Szostak E., Pocheć E., Michalik J.M., Piętosa J., Tahraoui T., Łuszczek M., Gondek Ł. Biocompatibility and potential functionality of lanthanum-substituted cobalt ferrite spinels, Journal of Alloys and Compounds, 2023; 966. 171433 https://doi.org/10.1016/j.jallcom.2023.171433
11. Winiarczyk K., Gac W., Góral-Kowalczyk M., Surowiec Z. Magnetic properties of iron oxide nanoparticles with a DMSA-modified surface, Hyperfine Interactions 2021; 242: 48, https://doi.org/10.1007/s10751-021-01768-w
12. Sharma S., Sharma H., Sharma R. A review on functionalization and potential application spectrum of magnetic nanoparticles (MNPs) based systems, Chemistry of Inorganic Materials 2024; 2: 100035, https://doi.org/10.1016/j.cinorg.2024.100035
13. Comanescu C. Recent advances in surface functionalization of magnetic nanoparticles. Coatings 2023; 13: 1772, https://doi.org/10.3390/coatings13101772
14. Hojnik Podrepšek G., Knez Ž., Leitgeb M. Development of chitosan functionalized magnetic nanoparticles with bioactive compounds. Nanomaterials 2020; 10: 1913, https://doi.org/10.3390/nano10101913
15. Pareek A., Alasiri G., Dudhwala Y., Alaseem A.M., Alsaidan O.A., Kapoor D.U. Prajapati BG. Review of engineered magnetic chitosan nanoparticles for drug delivery: Advances, challenges, and future prospects. Int J Biol Macromol. 2025; 327(Pt 2): 147441, https://doi.org/10.1016/j.ijbiomac.2025.147441
16. Pareek A., Alasiri G., Dudhwala Y., Alaseem A.M., Alsaidan O.A., Kapoor D.U., Prajapati B.G. Review of engineered magnetic chitosan nanoparticles for drug delivery: Advances, challenges, and future prospects. International Journal of Biological Macromolecules 2025; 327: 147441, https://doi.org/10.1016/j.ijbiomac.2025.147441
17. Sombut P., Gamba O., Meier M., Schmid M., Eder M., Diebold U., Angerler T., Franchini C. The surface phase diagram of Fe_3O_4(001) revisited, RSC Appl. Interfaces 2025; 2: 673, https://doi.org/10.1039/d5lf00022j
18. Queiroz M. F., Teodosio Melo K.R. Does the use of chitosan contribute to oxalate kidney stone formation?, Mar. Drugs 2015; 13: 141–158, https://doi.org/10.3390/md13010141
19. Rathinam K., Kou X., Hobby R., Panglisch S. Sustainable development of magnetic chitosan core–shell network for the removal of organic dyes from aqueous solutions. Materials 2021; 14: 7701, https://doi.org/10.3390/ma14247701
20. Fock, J., Hansen M.F., Frandsen C., Mørup, S. On the interpretation of Mössbauer spectra of magnetic nanoparticles. Journal of Magnetism and Magnetic Materials 2018; 445: 11–21, https://doi.org/10.1016/j.jmmm.2017.08.070
21. Wildeboer R.R., Southern P., Pankhurst Q.A. On the reliable measurement of specific absorption rates and intrinsic loss parameters in magnetic hyperthermia materials. J Phys D Appl Phys. 2014; 47: 495003, https://doi.org/10.1088/0022-3727/47/49/495003